available at www.sciencedirect.com

ScienceDirect

journal homepage: www.sciencedirect.com/journal/chinese-journal-of-catalysis

Article

Tuning the intermediate reaction barriers by a CuPd catalyst to improve the selectivity of CO_2 electroreduction to C2 products

Li Zhu [a], Yiyang Lin [a], Kang Liu [a], Emiliano Cortés [b], Hongmei Li [a], Junhua Hu [c], Akira Yamaguchi [d], Xiaoliang Liu [a,#], Masahiro Miyauchi [d,$], Junwei Fu [a,¥], Min Liu [a,*]

[a] *Shenzhen Research Institute, School of Physics and Electronics, Central South University, Changsha 410083, Hunan, China*
[b] *Chair in Hybrid Nanosystems, Nanoinstitute Munich, Faculty of Physics, Ludwig-Maximilians-Universität München, 80539 München, Germany*
[c] *School of Materials Science and Engineering, Zhengzhou University, Zhengzhou 450052, Henan, China*
[d] *Department of Materials Science and Engineering, School of Materials and Chemical Technology, Tokyo Institute of Technology, Tokyo 152-8552, Japan*

ARTICLE INFO

Article history:
Received 18 November 2020
Accepted 9 December 2020
Available online 5 May 2021

Keywords:
Carbon dioxide reduction
C2 products
Electrocatalyst
Copper-palladium interface
Intermediate reaction barriers

ABSTRACT

Electrochemical CO_2 reduction is a promising strategy for the utilization of CO_2 and intermittent excess electricity. Cu is the only single metal catalyst that can electrochemically convert CO_2 into multicarbon products. However, Cu exhibits an unfavorable activity and selectivity for the generation of C2 products because of the insufficient amount of CO* provided for the C-C coupling. Based on the strong CO_2 adsorption and ultrafast reaction kinetics of CO* formation on Pd, an intimate CuPd(100) interface was designed to lower the intermediate reaction barriers and improve the efficiency of C2 product formation. Density functional theory (DFT) calculations showed that the CuPd(100) interface enhanced the CO_2 adsorption and decreased the CO_2* hydrogenation energy barrier, which was beneficial for the C-C coupling. The potential-determining step (PDS) barrier of CO_2 to C2 products on the CuPd(100) interface was 0.61 eV, which was lower than that on Cu(100) (0.72 eV). Encouraged by the DFT calculation results, the CuPd(100) interface catalyst was prepared by a facile chemical solution method and characterized by transmission electron microscopy. CO_2 temperature-programmed desorption and gas sensor experiments further confirmed the enhancement of the CO_2 adsorption and CO_2* hydrogenation ability of the CuPd(100) interface catalyst. Specifically, the obtained CuPd(100) interface catalyst exhibited a C2 Faradaic efficiency of 50.3% ± 1.2% at −1.4 V_{RHE} in 0.1 M $KHCO_3$, which was 2.1 times higher than that of the Cu catalyst (23.6% ± 1.5%). This study provides the basis for the rational design of Cu-based electrocatalysts for the generation of multicarbon products by fine-tuning the intermediate reaction barriers.

1. Introduction

Excessive carbon emissions have caused serious global environmental issues [1–3]. The use of intermittent excess electricity to electrochemically convert CO_2 into valuable chemicals is a potential strategy to simultaneously solve the Earth's car-

* Corresponding author. Tel: +86-13787082527; E-mail: minliu@csu.edu.cn
# Corresponding author. E-mail: xl_liu@csu.edu.cn
$ Corresponding author. E-mail: mmiyauchi@ceram.titech.ac.jp
¥ Corresponding author. E-mail: fujunwei@csu.edu.cn

This work was supported by the Natural Science Foundation of China (21872174, 22002189, 51673217, U1932148), the International Science and Technology Cooperation Program (2017YFE0127800, 2018YFE0203402), the Hunan Provincial Science and Technology Program (2017XK2026), the Hunan Provincial Natural Science Foundation (2020JJ2041, 2020JJ5691), the Hunan Provincial Science and Technology Plan Project (2017TP1001), the Shenzhen Science and Technology Innovation Project (JCYJ20180307151313532).
DOI: 10.1016/S1872-2067(20)63754-8 | http://www.sciencedirect.com/science/journal/18722067 | Chin. J. Catal., Vol. 42, No. 9, September 2021

bon recycling and energy crises [4–8]. Among various CO_2 reduction products, C2 products (e.g., C_2H_4 and C_2H_5OH) have attracted much attention due to their higher energy density compared with C1 products (e.g., HCOOH and CH_4, CH_3OH) [9–11]. Cu is a unique single metal catalyst that can promote the electrochemical reduction of CO_2 to multicarbon (C_{2+}) products [12–14]. However, pure Cu catalysts lack the desirable activity and selectivity toward C2 products for practical applications [15,16]. The improvement of the efficiency of C2 product generation using Cu and Cu-based catalysts has aroused great interest [17–20].

There are two limiting factors for achieving the electroreduction of CO_2 to C2 products, namely the amount of CO* as carbon source (* indicates the adsorbate on the surface of a substrate) [21] and the C-C coupling step (two adjacent CO* coupling) [22,23]. For Cu catalysts, the energy barrier of the C-C coupling step is relatively low [24,25]. However, the CO_2 adsorption and CO_2* hydrogenation ability of Cu are unfavorable [26,27], resulting in an insufficient amount of adsorbed CO*. Therefore, different approaches have been explored to improve the catalytic activity of Cu for the generation of C2 products [28–30]. Among these, the design of Cu-based bimetallic catalysts is one of the most promising strategies [31–33]. In principle, a second metal component can effectively adjust the binding energy between the catalyst and intermediates [34–36], lower the energy barriers of intermediate reactions, and further increase the efficiency of C2 product formation [37,38]. Palladium is an efficient catalyst that exhibited strong CO_2 adsorption and ultrafast reaction kinetics for CO* formation. However, CO* poisoning on the Pd surface makes it unsuitable for generating C2 products [39]. To take full advantage of both Cu (C-C coupling) and Pd (CO* formation), the assembly of a CuPd bimetallic catalyst was envisaged as a potential method for optimizing the efficiency of C2 product formation.

In this study, we developed a CuPd(100) interface catalyst to tune the barriers of intermediate reaction and improve C2 product selectivity. Density functional theory (DFT) calculations predicted that the CuPd(100) interface could more strongly adsorb CO_2 and dramatically decrease the energy barrier of CO_2* hydrogenation compared with the Cu(100) facet, leading to sufficient CO* for the later C-C coupling step. The calculated potential-determining step (PDS) of CO_2 conversion to C2 products in the presence of the CuPd(100) interface was a C-C coupling with an energy barrier of 0.61 eV, which was much lower than that of 0.72 eV observed for the PDS (CO_2* hydrogenation) using Cu(100), indicating a potentially higher efficiency of C2 product formation in the case of the CuPd(100) interface catalyst. Experimentally, the CuPd(100) interface catalyst was prepared using an in-situ growth method based on thermal reduction to afford Pd nanoparticles (NPs) as nucleation seeds. The obtained CuPd(100) interface catalyst was characterized using X-ray diffraction (XRD), transmission electron microscopy (TEM), and X-ray photoelectron spectroscopy (XPS) analyses. The enhancement of CO_2 adsorption and CO_2* hydrogenation abilities on the CuPd(100) interface were demonstrated by performing CO_2-TPD and gas sensor experiments, respectively. Specifically, the CuPd(100) interface catalyst exhibited a C2 Faradaic efficiency (FE) of 50.3% ± 1.2% at −1.4 V_{RHE} in 0.1 M $KHCO_3$, which was 2.1 times higher than that of the parent Cu catalyst (23.6% ± 1.5%). This study provides a strategy to improve the yield of target C2 products by regulating the energy barrier of the intermediate reactions as well as a reference for the development of Cu-based catalysts with higher efficiency for the generation of multicarbon products.

2. Experimental

2.1. DFT calculations

To explore the mechanism of the CO_2 conversion to C2 products, 4 × 2 Cu(100), Pd(100), and CuPd(100) periodic surface slabs with four atomic layers were built, as shown in Fig. S1. Main consideration is that the Cu(100) facet favored the formation of C2 products [40,41]. A vacuum slab of 30 Å was added to avoid the interaction influence of the periodic boundary conditions. Each model contained 128 atoms. Potassium (K) ions not only promote the activation of CO_2 [42], but also lower the energy barrier of the C-C coupling [24]. Thus, six K ions were added to the model to simulate the actual CO_2 reduction process.

DFT calculations were performed by VASP with the projector augment wave (PAW) method [43,44]. The exchange and correlation potentials were present in the generalized gradient approximation in combination with the Perdew-Burke- Ernzerhof correlation (GGA-PBE) [45,46]. A 2 × 2 × 1 gamma grid of k-points was used for the Brillouin zone integration. The cutoff energy as well as convergence criteria for energy and force were set as 450 eV, 10^{-5} eV/atom, and 0.02 eV/Å, respectively.

The adsorption energy was calculated according to the following Eq. (1) [47,48]:

$$E_{ads} = E_{substrate+gas} - (E_{substrate} + E_{gas}) \quad (1)$$

where $E_{substrate}$ and E_{gas} represent the energy of the isolated substrate and gas molecule, respectively, while $E_{substrate+gas}$ represents the total energy of the gas molecule adsorbed on the substrate. Herein, the substrates refer to the Cu(100), Pd(100), and CuPd(100) interfaces.

The change in Gibbs free energy (ΔG) for each reaction step is given as follows [49,50]:

$$\Delta G = \Delta E + \Delta ZPE - T\Delta S \quad (2)$$

where ΔE represents the total energy difference between the product and reactant, while ΔZPE and $T\Delta S$ indicate the zero-point energy correction and entropy change at 298.15 K, respectively.

2.2. Catalyst synthesis

Preparation of the Cu sample: 3 mmol of copper acetate was thoroughly dissolved in 250 mL of 2-ethoxyethanol under vigorous stirring and Ar bubbling. After 30 min, 20 mL of aq. $NaBH_4$ (1.5 M) was added dropwise to the above solution. The obtained black precipitate was washed several times with water and ethanol. The collected Cu sample was dried at 60 °C for 6 h in vacuum, and then dispersed in isopropyl alcohol [51].

Preparation of the Pd sample: 3 mmol of palladium acetate was first dissolved in 30 mL of acetone, and then 250 mL of 2-ethoxyethanol was added. Then, 20 mL of aq. $NaBH_4$ (1.5 M) was added dropwise to the mixture. The obtained black precipitate was washed with water and ethanol several times, dried at 60 °C for 6 h in vacuum, and then dispersed in isopropyl alcohol.

Preparation of the CuPd sample: 1.5 mmol of palladium acetate was dissolved in 10 mL of acetone. Next, 250 mL of 2-ethoxyethanol was added, and the mixture was heated at 393 K for 30 min under vigorous stirring and Ar bubbling. After cooling to room temperature, 20 mL of copper acetate aqueous solution (75 mmol/L) was added dropwise with stirring, followed by 20 mL of $NaBH_4$ aqueous solution (1.5 M). The obtained black precipitate was thoroughly washed with water and ethanol, dried at 60 °C for 6 h in vacuum, and then dispersed in isopropyl alcohol.

3. Results and discussion

The adsorption energy of CO_2 and ΔG of CO_2* hydrogenation are shown in Figs. 1(a,b), respectively [19,36,52–54]. The adsorption energy of CO_2 in the case of the CuPd(100) interface (−0.72 eV) was higher than that of Cu(100) (−0.45 eV) but lower than that of Pd(100) (−0.91 eV). Fig. S3 shows that the adsorption of CO_2 on these models without K^+ was much weaker than in the presence of K^+. It can be inferred that CO_2 adsorption was strongly enhanced by the presence of K^+ [42]. The ΔG of the CO_2* hydrogenation in the presence of the CuPd(100) interface greatly decreased to 0.13 eV from 0.72 eV in the case of Cu(100), while being even lower than that on Pd(100) (0.40 eV). Considering that the zero-point energy and entropy energy correction were extremely small, the ΔG of the CO_2* hydrogenation mainly depended on the difference between $E_{substrate+COOH*}$ and $E_{substrate+CO2*}$. The more negative the $E_{substrate+COOH*}$ (the stronger the COOH* adsorption on the substrate) and the more positive the $E_{substrate+CO2*}$ (the weaker CO_2* adsorption on the substrate), the smaller is the ΔG of the CO_2* hydrogenation. Therefore, the dramatic decrease in ΔG of the CO_2* hydrogenation on the CuPd(100) interface could be attributed to a strong COOH* adsorption and appropriate CO_2 adsorption of the CuPd(100) interface (Figs. S2 and S3).

Fig. S5(a) shows the adsorption energy of CO* on Cu(100), CuPd(100) interface, and Pd(100) facet with K ions to be −1.2, −2, and −2.4 eV, respectively. Thus, a higher amount of CO* is formed on the CuPd(100) interface compared with that on the Cu(100) facet, leading to an increased chance of the C-C coupling step occurring. In addition, the adsorption energies of CO* relative to different CO* coverages on the Pd(100) facet are shown in Fig. S5(b). These results demonstrated that adsorption of CO* on Pd(100) decreased as the CO* coverage increased, which indicates that CO* desorption from Pd is possible at high CO* coverages [55].

Fig. S6 shows that the energy barriers of the two CO* couplings in the presence of Cu(100) and CuPd(100) were lower than that of the CO* hydrogenation. Therefore, it can be assumed that the C-C coupling step using Cu(100) and CuPd(100) involved two CO* couplings rather than two COH*/CHO* coupling. The obtained free energies of the two CO* coupling on the Cu(100), CuPd(100), and Pd(100) facet were 0.09, 0.61, and 1.44 eV, respectively (Fig. 1(b)). The large ΔG observed for the Pd(100) facet was consistent with previously reported results, proving that Pd did not exert catalytic activity for C2 product generation.

As previously reported, the PDS step of the CO_2 electroreduction to C2 products was either the CO_2 activation or C-C

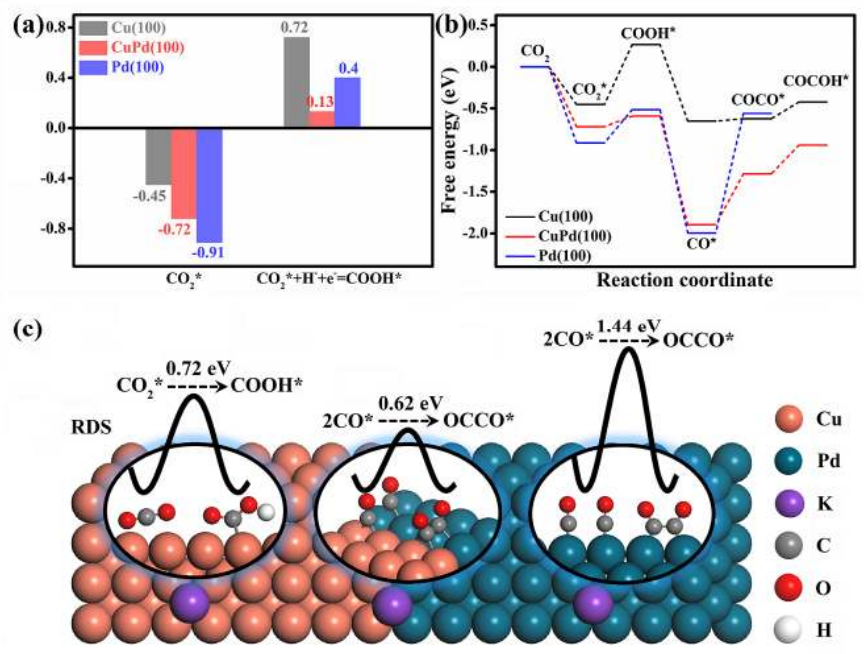

Fig. 1. (a) Adsorption energy of CO_2 and ΔG of CO_2* hydrogenation; (b) Calculated free energy diagrams for the CO_2 reduction process; (c) Schematic diagram of the PDS of the CO_2 reduction process on Cu(100), CuPd(100) interface, and Pd(100) facet.

coupling [40]; therefore, it was suggested that the PDS of the CO_2 reduction to C2 products using the CuPd(100) interface was a C-C coupling with an energy barrier of 0.61 eV, which was less than 0.72 eV for the CO_2* hydrogenation on Cu(100). Therefore, the CuPd(100) interface was more effective in facilitating the conversion of CO_2 to C2 products compared with the Cu(100) facet.

Encouraged by these predictions, we prepared the Cu, CuPd, and Pd samples using a thermal reduction treatment followed by an in situ growth process. As shown in Fig. S4, the XRD patterns indicated that the CuPd sample before electrochemical reduction contained the characteristic peaks of Cu (PDF No. 03-1015), Pd (PDF No. 05-0681), and Cu_2O (PDF No. 78-0428). After electrochemical reduction for 30 min, the characteristic Cu_2O peak disappeared (Fig. 2(a)). These results revealed that the effect of the oxidation state of Cu on the catalytic activity of these catalysts was negligible, and the CuPd sample consisted of separate Cu and Pd phases rather than a CuPd alloy [51,56]. Fig. 2(b) shows the TEM image of the CuPd sample, which exhibited a typical nanoparticle morphology with a size of approximately 20 nm. The high-resolution TEM (HRTEM) image (Fig. 2(c)) shows lattice distances of 0.182 and 0.194 nm, which corresponded to the Cu(100) and Pd(100) facets, respectively [29], while the red line shows a clear CuPd(100) interface. Fig. 2(d) shows the HAADF-STEM and EDS mapping images, demonstrating the separate distribution of the Cu (green) and Pd (red) phases. The TEM and HRTEM images of the Cu and Pd samples are shown in Fig. S5; the lattice distances of 0.181 and 0.195 nm corresponded to the Cu(100) facet of the Cu sample and Pd(100) facet of the Pd sample, respectively.

XPS was further used to study the composition and elemental chemical state of the samples [57–59]. As shown in Figs. 3(a,b), the Cu 2*p* binding energy of the CuPd sample exhibited a 0.2 eV positive shift compared with the Cu sample, while its Pd 3*d* binding energy moved by 0.16 eV toward the low energy region compared with in case of the Pd sample. The slight shifts in the binding energies of Cu 2*p* and Pd 3*d* indicated an electron transfer from Cu to Pd, revealing an intimate interaction between Cu and Pd in the CuPd sample [30]. Figs. 3(c,d) show the Cu *K*- and Pd *K*-edge extended X-ray absorption fine structure (EXAFS) spectra of the CuPd sample. Only the Cu-Cu and Pd-Pd bonds are visible in the spectra. The XPS and EXAFS results together with those of the XRD and TEM analyses clearly demonstrated that the obtained CuPd catalyst consisted of a phase-separated sample with CuPd(100) interfaces.

To characterize the CO_2 adsorption ability of the three catalysts, CO_2-TPD measurements and thermogravimetric experiments were carried out (Fig. 4(a) and Fig. S6). The main CO_2 desorption peak of the Cu catalyst was located at 296 °C [60], while that of the Pd catalyst was positioned at 608 °C [61]. In contrast, three main CO_2 desorption peaks at 288, 355, and 598 °C were observed for the CuPd(100) interface catalyst. Unlike the Cu and Pd catalysts, the peak located at 355 °C could be assigned to the CuPd(100) interface, suggesting a stronger and weaker CO_2 adsorption than that on Cu and Pd, respectively.

To prove the strong COOH* adsorption ability of the CuPd(100) interface catalyst, we designed a gas sensor experiment (Fig. S7) [62,63]. Fig. 4(c) shows the current density curves of the Cu, CuPd(100) interface, and Pd catalysts at different applied potentials under vacuum and saturated CO_2+H_2O atmosphere. Fig. 4(d) shows the calculated current density differences (Δj) between the vacuum and CO_2+H_2O atmosphere. The higher the value of Δj, the stronger is the adsorption of CO_2 and H_2O, which is an important indicator of COOH* adsorption. These results shows that the CuPd(100) interface catalyst displayed the strongest COOH* adsorption ability.

Furthermore, CO-TPD was used to investigate the CO adsorption ability of these three catalysts [64,65]. As shown in Fig. 4(b), the CuPd(100) interface catalyst exhibited three evident desorption peaks located at 204, 271, and 529 °C. On the other hand, the reference catalysts Cu and Pd showed desorption peaks at 211 and 609 °C, respectively [66,67]. In combination with the three CO desorption curves, the peak at 271 °C could be ascribed to the contribution of the CuPd(100) inter-

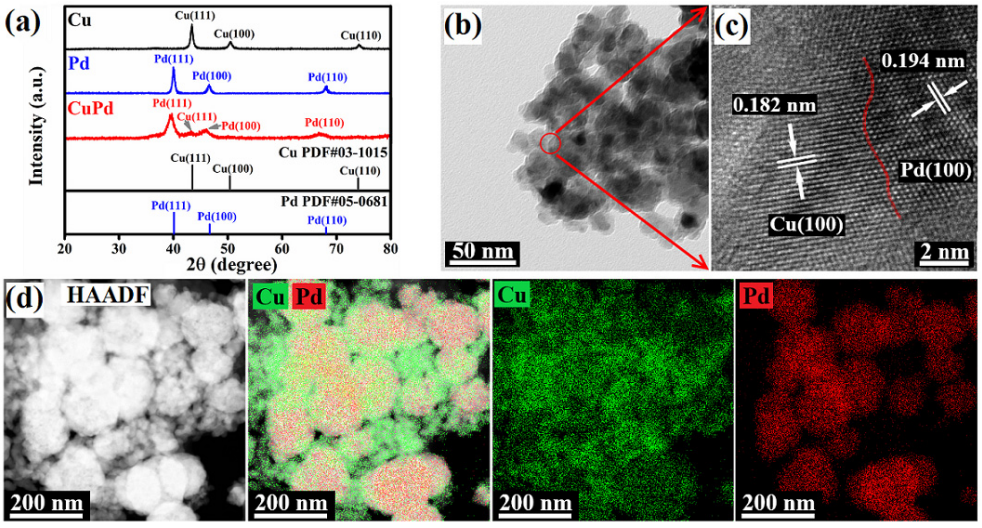

Fig. 2. (a) XRD patterns of the prepared Cu, CuPd, and Pd samples after electrochemical reduction for 30 min; (b,c) Low-resolution and high-resolution TEM images of the CuPd sample; (d) HAADF-STEM image combined with the EDS mapping of the CuPd sample.

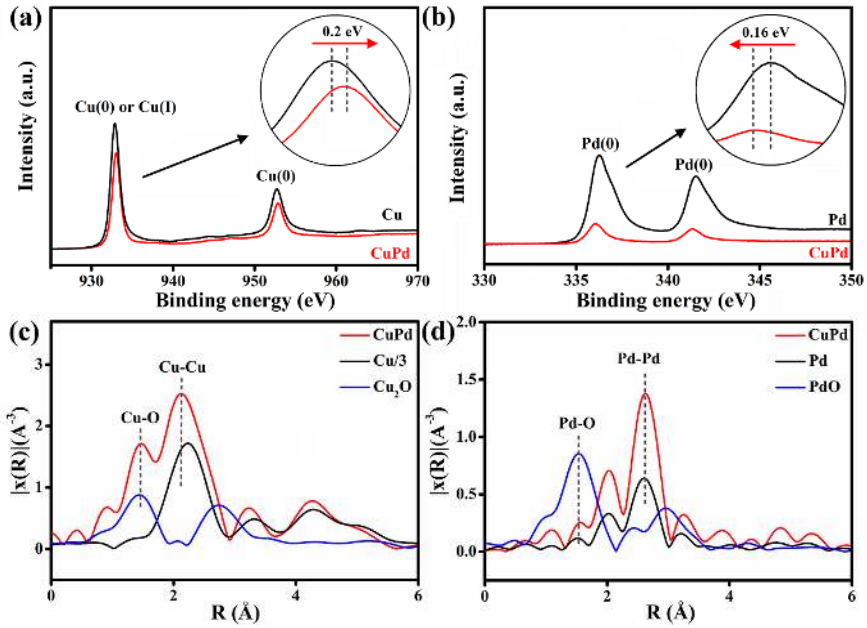

Fig. 3. XPS spectra of Cu 2*p* (a) and Pd 3*d* (b); EXAFS spectra of Cu *K*-edge (c) and Pd *K*-edge (d) of the CuPd sample.

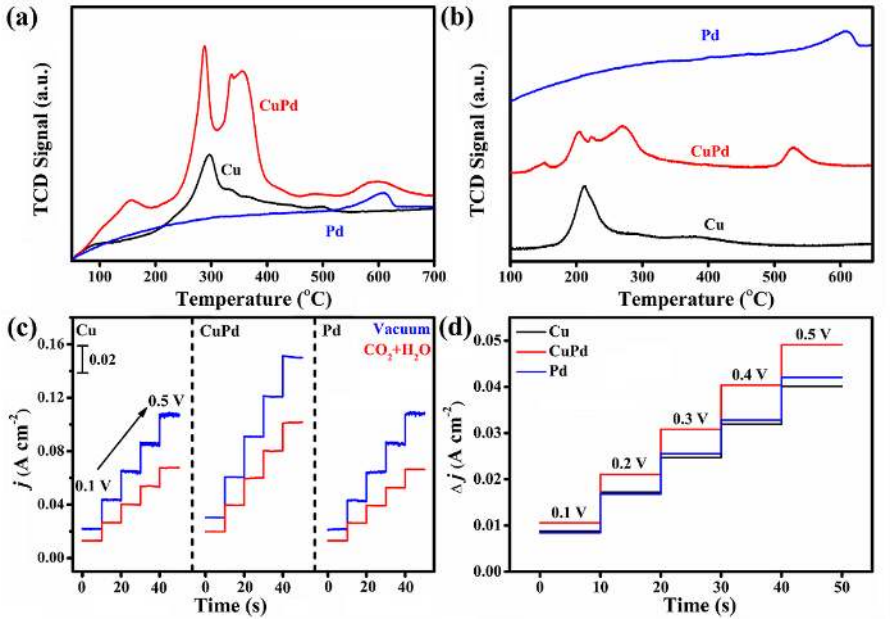

Fig. 4. CO_2-TPD (a) and CO-TPD (b) curves of Cu, CuPd(100) interface, and Pd catalysts; (c) Gas sensor experiments for Cu, CuPd(100) interface, and Pd catalysts at 0.1, 0.2, 0.3, 0.4, and 0.5 V; (d) Calculated current density differences (Δ*j*) between vacuum and CO_2+H_2O atmosphere.

face. The moderate desorption temperature (271 °C) of the CuPd(100) interface compared with Cu (204 °C) and Pd (609 °C) suggested a moderate CO adsorption ability of the CuPd(100) interface.

To assess the catalytic activity of the CuPd(100) interface catalyst, a CO_2 electroreduction test was performed. As shown in Fig. 5(a), for the Cu catalyst, the FE of C2 products gradually increased from 3.7% ± 0.4% to 23.6% ± 1.5% at a cathode potential ranging from −0.8 to −1.4 V_{RHE}, while the FE of C1 products accordingly decreased from 54.7% ± 1.3% to 30.6% ± 1.4% within the same potential range. For the CuPd(100) interface catalyst, the FE of C2 products increased from 7% ± 0.6% to 50.3% ± 1.2% at the corresponding potentials, which was 2.1 times higher than that of the Cu catalyst (23.6% ± 1.5%). For the Pd catalyst, only C1 products and H_2 were detected, and the FE of H_2 gradually increased as the cathode potential increased negatively. More detailed data on the FE of the products of these three catalysts are shown in Fig. S8.

To analyze the selectivity of C2 products, the FE ratios of C2 to C1 products (FE_{C2}/FE_{C1}) at different applied potentials were determined, as shown in Fig. 5(b). At all applied potentials, the FE_{C2}/FE_{C1} of the CuPd(100) interface catalyst was larger than that of the Cu catalyst. In particular, at −1.4 V_{RHE} the FE_{C2}/FE_{C1} of the CuPd(100) interface catalyst reached 2.4, while that of the Cu catalyst was 0.77. This result proved a higher selectivity toward C2 products of the CuPd(100) interface catalyst than

that of the Cu catalyst. As previously mentioned, C2 products were not detected in the presence of the Pd catalyst.

Fig. 5(c) shows the current densities at different cathode potentials. The current density of the CuPd(100) interface catalyst was significantly greater than that of the Cu and Pd catalysts at each potential, indicating faster reaction kinetics for the CuPd(100) interface catalyst. This performance was also confirmed by linear sweep voltammetry (LSV) curves (Fig. S9). Moreover, the CuPd(100) interface catalyst displayed the lowest Tafel slope (374 mV dec^{-1}) compared with the Cu (384 mV dec^{-1}) and Pd (467 mV dec^{-1}) catalyst (Fig. 5(d)), demonstrating rapid C2 product generation kinetics in the presence of the CuPd(100) interface.

Furthermore, electrochemically active surface area (ECSA) tests showed that the CuPd(100) interface catalyst possessed the highest ECSA (7.04×10^{-3} mF cm^{-2}), followed by the Cu (1.84×10^{-3} mF cm^{-2}) and Pd catalyst (0.99×10^{-3} mF cm^{-2}) (Fig. S10). The electrochemical impedance spectra (EIS) show that the CuPd(100) interface catalyst possessed the best electrical conductivity among the three catalysts (Fig. S11). These results proved that the CuPd(100) interface catalyst displayed a greater activity and selectivity toward C2 products than both Cu and Pd catalysts.

4. Conclusions

In summary, DFT calculations predicted that a CuPd(100) interface catalyst could possess a higher efficiency for the generation of C2 products during a CO_2 electroreduction reaction compared with that of Cu or Pd monometallic catalysts. These calculations showed that the CuPd(100) interface catalyst could provide sufficient CO* for the C-C coupling by enhancing the CO_2 adsorption and decreasing the energy barrier of the CO_2* hydrogenation step. The PDS energy barrier of CO_2 conversion to C2 products on the CuPd(100) interface catalyst (0.61 eV) was smaller than that of Cu(100) (0.72 eV). Guided by these theoretical predictions, the CuPd(100) interface catalyst was synthesized using a thermal reduction treatment followed by an in-situ growth process. The CuPd(100) interface was clearly visible in the corresponding HRTEM image. By combining the CO_2-TPD results and gas sensor measurements, the enhanced adsorption of CO_2 along with the decrease in the energy barrier of the CO_2* hydrogenation on the CuPd(100) interface were further verified. Specifically, the CuPd(100) interface catalyst exhibited a C2 FE of 50.3% ± 1.2% at −1.4 V_{RHE} in 0.1 M $KHCO_3$, which was 2.1 times higher than that of the Cu catalyst (23.6% ± 1.5%). The consistency between the theoretical and experimental results provided new insights into the design of superior Cu-based electrocatalysts for the conversion of CO_2 to desired multicarbon products.

Conflicts of interest

There are no conflicts to declare.

Author contributions

Min Liu, Junwei Fu, Masahiro Miyauchi and Xiaoliang Liu supervised the project. Min Liu and Akira Yamaguchi designed the experiments and analysed the results. Li Zhu synthesized the samples, performed the electrochemical experiments, and analysed the results. Li Zhu and Kang Liu carried out the DFT calculation and wrote the corresponding section. Yiyang Lin, Ying-Rui Lu and Ting-Shan Chan conducted the EXAFS measurements, and Emiliano Cortés analysed the results. Junhua Hu and Hongmei Li carried out the electron microscope measurements. All authors read and commented on the manuscript.

Acknowledgments

The authors gratefully thank the Natural Science Foundation of China (21872174, 22002189, 51673217, U1932148), the

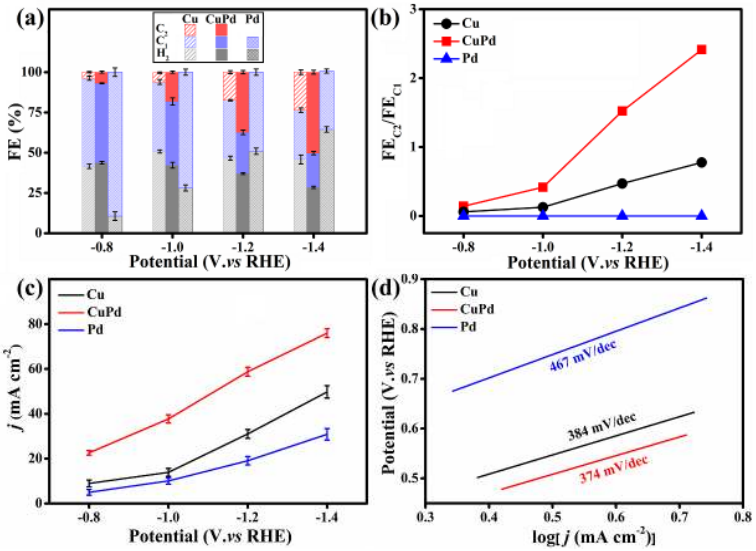

Fig. 5. (a) FE of different products for Cu, CuPd(100) interface, and Pd catalysts at different applied potentials; (b) FE ratios of C2 to C1 products (FE_{C2}/FE_{C1}) at different applied potentials; (c) Current density curves and (d) Tafel slopes for Cu, CuPd(100) interface, and Pd catalysts.

International Science and Technology Cooperation Program (2017YFE0127800, 2018YFE0203402), the Hunan Provincial Science and Technology Program (2017XK2026), the Hunan Provincial Natural Science Foundation (2020JJ2041, 2020JJ5691), the Hunan Provincial Science and Technology Plan Project (2017TP1001), the Shenzhen Science and Technology Innovation Project (JCYJ20180307151313532), Ministry of Science and Technology, Taiwan, China (MOST108-2113-M-213-006). Emiliano Cortés acknowledges funding and support from the Deutsche Forschungsgemeinschaft (DFG, German Research Foundation) under Germany´s Excellence Strategy (EXC 2089/1-390776260), the Bavarian Solar Energies Go Hybrid (SolTech) program and the Center for NanoScience (CeNS), the European Commission for the ERC Starting Grant CATALIGHT (802989).

Electronic supporting information

Supporting information is available in the online version of this article.

References

[1] X. Lim, *Nature*, **2015**, 526, 628–630.
[2] O. S. Bushuyev, P. De Luna, C. T. Dinh, L. Tao, G. Saur, J. van de Lagemaat, S. O. Kelley, E. H. Sargent, *Joule*, **2018**, 2, 825–832.
[3] X. Wang, Y. Wang, X. Sang, W. Zheng, S. Zhang, L. Shuai, B. Yang, Z. Li, J. Chen, L. Lei, N. M. Adli, M. K. H. Leung, M. Qiu, G. Wu, Y. Hou, *Angew. Chem. Int. Ed.*, **2020**, 10.1002/anie.202013427.
[4] J. Fu, S. Wang, Z. Wang, K. Liu, H. Li, H. Liu, J. Hu, X. Xu, H. Li, M. Liu, *Front. Phys.*, **2020**, 15, 33201.
[5] G. Yang, Z. Yu, J. Zhang, Z. Liang, *Chin. J. Catal.*, **2018**, 39, 914–919.
[6] J. Hao, W. Shi, *Chin. J. Catal.*, **2018**, 39, 1157–1166.
[7] C. Yan, L. Lin, G. Wang, X. Bao, *Chin. J. Catal.*, **2019**, 40, 23–37.
[8] S. Feng, W. Zheng, J. Zhu, Z. Li, B. Yang, Z. Wen, J. Lu, L. Lei, S. Wang, Y. Hou, *Appl. Catal. B*, **2020**, 270, 118908.
[9] J. Fu, K. Jiang, X. Qiu, J. Yu, M. Liu, *Mater. Today*, **2020**, 32, 222–243.
[10] J. Shao, Y. Wang, D. Gao, K. Ye, Q. Wang, G. Wang, *Chin. J. Catal.*, **2020**, 41, 1393–1400.
[11] T. Wang, X. Sang, W. Zheng, B. Yang, S. Yao, C. Lei, Z. Li, Q. He, J. Lu, L. Lei, L. Dai, Y. Hou, *Adv. Mater.*, **2020**, 32, 2002430.
[12] Y. Chen, K. Chen, J. Fu, A. Yamaguchi, H. Li, H. Pan, J. Hu, M. Miyauchi, M. Liu, *Nano Mater. Sci.*, **2020**, 2, 235–247.
[13] H. Zhou, K. Liu, H. Li, M. Cao, J. Fu, X. Gao, J. Hu, W. Li, H. Pan, J. Zhan, Q. Li, X. Qiu, M. Liu, *J. Colloid Interface Sci.*, **2019**, 550, 17–47.
[14] Y. Zhou, F. Che, M. Liu, C. Zou, Z. Liang, P. De Luna, H. Yuan, J. Li, Z. Wang, H. Xie, H. Li, P. Chen, E. Bladt, R. Quintero-Bermudez, T. K. Sham, S. Bals, J. Hofkens, D. Sinton, G. Chen, E. H. Sargent, *Nat. Chem.*, **2018**, 10, 974–980.
[15] S. Jia, Q. Zhu, H. Wu, M. Chu, S. Han, R. Feng, J. Tu, J. Zhai, B. Han, *Chin. J. Catal.*, **2020**, 41, 1091–1098.
[16] W. Xiong, J. Yang, L. Shuai, Y. Hou, M. Qiu, X. Li, M. K. H. Leung, *ChemElectroChem*, **2019**, 6, 5951–5957.
[17] P. An, L. Wei, H. Li, B. Yang, K. Liu, J. Fu, H. Li, H. Liu, J. Hu, Y. R. Lu, H. Pan, T.-S. Chan, N. Zhang, M. Liu, *J. Mater. Chem. A*, **2020**, 8, 15936–15941.
[18] J. Wang, Z. Li, C. Dong, Y. Feng, J. Yang, H. Liu, X. Du, *ACS Appl. Mater. Interfaces*, **2019**, 11, 2763–2767.
[19] M. Xing, L. Guo, Z. Hao, *Dalton Trans.*, **2019**, 48, 1504–1515.
[20] H. Xiao, W. A. Goddard III, T. Cheng, Y. Liu, *Proc. Natl. Acad. Sci. USA*, **2017**, 114, 6685–6688.
[21] L. Ou, Y. Chen, J. Jin, *Chem. Phys. Lett.*, **2018**, 710, 175–179.
[22] G. Mangione, J. Huang, R. Buonsanti, C. Corminboeuf, *J. Phys. Chem. Lett.*, **2019**, 10, 4259–4265.
[23] J. H. Montoya, C. Shi, K. Chan, J. K. Norskov, *J. Phys. Chem. Lett.*, **2015**, 6, 2032–2037.
[24] E. Perez-Gallent, G. Marcandalli, M. C. Figueiredo, F. Calle-Vallejo, M. T. M. Koper, *J. Am. Chem. Soc.*, **2017**, 139, 16412–16419.
[25] T. K. Todorova, M. W. Schreiber, M. Fontecave, *ACS Catal.*, **2019**, 10, 1754–1768.

Graphical Abstract

Chin. J. Catal., 2021, 42: 1500–1508 doi: 10.1016/S1872-2067(20)63754-8

Tuning the intermediate reaction barriers by a CuPd catalyst to improve the selectivity of CO_2 electroreduction to C2 products

Li Zhu, Yiyang Lin, Kang Liu, Emiliano Cortés, Hongmei Li, Junhua Hu, Akira Yamaguchi, Xiaoliang Liu *, Masahiro Miyauchi *, Junwei Fu *, Min Liu *
Central South University, China; Ludwig-Maximilians-Universität München, Germany; Zhengzhou University, China; Tokyo Institute of Technology, Japan

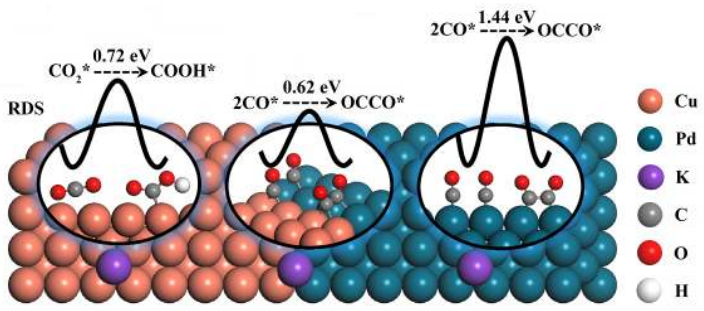

A CuPd(100) catalyst was designed and fabricated to improve the selectivity of the electroreduction of CO_2 to C2 products by tuning the CO_2 adsorption ability and intermediate reaction barriers.

[26] T. Cheng, H. Xiao, W. A. Goddard III, *J. Am. Chem. Soc.*, **2016**, 138, 13802–13805.
[27] L. Ou, *RSC Adv.*, **2015**, 5, 57361–57371.
[28] S. Bai, Q. Shao, P. Wang, Q. Dai, X. Wang, X. Huang, *J. Am. Chem. Soc.*, **2017**, 139, 6827–6830.
[29] J. Gao, H. Zhang, X. Guo, J. Luo, S. M. Zakeeruddin, D. Ren, M. Gratzel, *J. Am. Chem. Soc.*, **2019**, 141, 18704–18714.
[30] J. Huang, M. Mensi, E. Oveisi, V. Mantella, R. Buonsanti, *J. Am. Chem. Soc.*, **2019**, 141, 2490–2499.
[31] L. Lu, X. Sun, J. Ma, D. Yang, H. Wu, B. Zhang, J. Zhang, B. Han, *Angew. Chem. Int. Ed.*, **2018**, 57, 14149–14153.
[32] Z. Weng, X. Zhang, Y. Wu, S. Huo, J. Jiang, W. Liu, G. He, Y. Liang, H. Wang, *Angew. Chem. Int. Ed.*, **2017**, 56, 13135–13139.
[33] W. Zhu, L. Zhang, P. Yang, X. Chang, H. Dong, A. Li, C. Hu, Z. Huang, Z. J. Zhao, J. Gong. *Small*, **2018**, 14, 1703314.
[34] D. Chen, Q. Yao, P. Cui, H. Liu, J. Xie, J. Yang, *ACS Appl. Energy Mater.*, **2018**, 1, 883–890.
[35] L. Liu, F. Fan, Z. Jiang, X. Gao, J. Wei, T. Fang, *J. Phys. Chem. C*, **2017**, 121, 26287–26299.
[36] X. Nie, X. Jiang, H. Wang, W. Luo, M. J. Janik, Y. Chen, X. Guo, C. Song, *ACS Catal.*, **2018**, 8, 4873–4892.
[37] C. S. Chen, J. H. Wan, B. S. Yeo, *J. Phys. Chem. C*, **2015**, 119, 26875–26882.
[38] S. Lee, G. Park, J. Lee, *ACS Catal.*, **2017**, 7, 8594–8604.
[39] D. Gao, H. Zhou, F. Cai, J. Wang, G. Wang, X. Bao, *ACS Catal.*, **2018**, 8, 1510–1519.
[40] W. Luo, X. Nie, M. J. Janik, A. Asthagiri, *ACS Catal.*, **2015**, 6, 219–229.
[41] E. Perez-Gallent, M. C. Figueiredo, F. Calle-Vallejo, M. T. M. Koper, *Angew. Chem. Int. Ed.*, **2017**, 56, 3621–3624.
[42] M. Liu, Y. Pang, B. Zhang, P. De Luna, O. Voznyy, J. Xu, X. Zheng, C. T. Dinh, F. Fan, C. Cao, F. P. de Arquer, T. S. Safaei, A. Mepham, A. Klinkova, E. Kumacheva, T. Filleter, D. Sinton, S. O. Kelley, E. H. Sargent, *Nature*, **2016**, 537, 382–386.
[43] G. Kresse, J. Furthmüller, *Phys. Rev. B*, **1996**, 54, 11169–11186.
[44] G. Kresse, D. Joubert, *Phys. Rev. B*, **1999**, 59, 1758–1775.
[45] J. P. Perdew, K. Burke, M. Ernzerhof, *Phys. Rev. Lett.*, **1996**, 77, 3865–3868.
[46] J. P. Perdew, Y. Wang, *Phys. Rev. B*, **1992**, 45, 13244–13249.
[47] H. J. W. Li, H. Zhou, K. Chen, K. Liu, S. Li, K. Jiang, W. Zhang, Y. Xie, Z. Cao, H. Li, H. Liu, X. Xu, H. Pan, J. Hu, D. Tang, X. Qiu, J. Fu, M. Liu, *Solar RRL*, **2020**, 4, 1900416.
[48] Y. Huo, J. Zhang, K. Dai, Q. Li, J. Lv, G. Zhu, C. Liang, *Appl. Catal. B*, **2019**, 241, 528–538.
[49] K. Liu, J. Fu, L. Zhu, X. Zhang, H. Li, H. Liu, J. Hu, M. Liu, *Nanoscale*, **2020**, 12, 4903–4908.
[50] M. Liu, M. Liu, X. Wang, S. M. Kozlov, Z. Cao, P. De Luna, H. Li, X. Qiu, K. Liu, J. Hu, C. Jia, P. Wang, H. Zhou, J. He, M. Zhong, X. Lan, Y. Zhou, Z. Wang, J. Li, A. Seifitokaldani, C. T. Dinh, H. Liang, C. Zou, D. Zhang, Y. Yang, T. S. Chan, Y. Han, L. Cavallo, T. K. Sham, B. J. Hwang, E. H. Sargent, *Joule*, **2019**, 3, 1703–1718.
[51] S. Ma, M. Sadakiyo, M. Heima, R. Luo, R. T. Haasch, J. I. Gold, M. Yamauchi, P. J. A. Kenis, *J. Am. Chem. Soc.*, **2017**, 139, 47–50.
[52] W. Ju, A. Bagger, X. Wang, Y. Tsai, F. Luo, T. Möller, H. Wang, J. Rossmeisl, A. S. Varela, P. Strasser, *ACS Energy Lett.*, **2019**, 4, 1663–1671.
[53] Y. Jiao, Y. Zheng, P. Chen, M. Jaroniec, S. Z. Qiao, *J. Am. Chem. Soc.*, **2017**, 139, 18093–18100.
[54] A. A. Peterson, J. K. Nørskov, *J. Phys. Chem. Lett.*, **2012**, 3, 251–258.
[55] H. Liu, J. Liu, B. Yang, *Phys. Chem. Chem. Phys.*, **2020**, 22, 9600–9606.
[56] X. Liu, Q. Han, Y. Liu, C. Xie, C. Yang, D. Niu, Y. Li, H. Wang, L. Xia, Y. Yuan, Y. Gao, *Appl. Phys. Lett.*, **2020**, 116, 253303.
[57] K. Chen, W. Fan, C. Huang, X. Qiu, *J. Phys. Chem. Solids*, **2017**, 110, 9–14.
[58] K. Chen, H. Li, Y. Xu, K. Liu, H. Li, X. Xu, X. Qiu, M. Liu, *Nanoscale*, **2019**, 11, 5967–5973.
[59] P. Liu, X. Liu, L. Lyu, H. Xie, H. Zhang, D. Niu, H. Huang, C. Bi, Z. Xiao, J. Huang, Y. Gao, *Appl. Phys. Lett.*, **2015**, 106, 193903.
[60] L. Frusteri, C. Cannilla, S. Todaro, F. Frusteri, G. Bonura, *Catalysts*, **2019**, 9, 1058.
[61] X. Zhang, X. Chen, Y. Liu, M. Guo, *Water Air Soil Pollut.*, **2020**, 231, 277.
[62] S. Cao, Y. Chen, H. Wang, J. Chen, X. Shi, H. Li, P. Cheng, X. Liu, M. Liu, L. Piao, *Joule*, **2018**, 2, 549–557.
[63] K. Chen, K. Liu, P. An, H. Li, Y. Lin, J. Hu, C. Jia, J. Fu, H. Li, H. Liu, Z. Lin, W. Li, J. Li, Y. R. Lu, T. S. Chan, N. Zhang, M. Liu, *Nat. Commun.*, **2020**, 11, 4173.
[64] J. Fu, K. Liu, K. Jiang, H. Li, P. An, W. Li, N. Zhang, H. Li, X. Xu, H. Zhou, D. Tang, X. Wang, X. Qiu, M. Liu, *Adv. Sci.*, **2019**, 6, 1900796.
[65] K. Jiang, L. Zhu, Z. Wang, K. Liu, H. Li, J. Hu, H. Pan, J. Fu, N. Zhang, X. Qiu, M. Liu, *Appl. Surf. Sci.*, **2020**, 508, 145173.
[66] J. Butorac, E. L. Wilson, H. H. Fielding, W. A. Brown, R. S. Minns, *RSC Adv.*, **2016**, 6, 66346–66359.
[67] A. Kokalj, T. Makino, M. Okada, *J. Phys.: Condens. Matter*, **2017**, 29, 194001.

CuPd催化剂调节中间反应能垒提高电催化CO_2生成二碳产物的选择性

朱　莉[a], 林翌阳[a], 刘　康[a], Emiliano Cortés [b], 李红梅[a], 胡俊华[c], Akira Yamaguchi [d], 刘小良[a,#], Masahiro Miyauchi [d,$], 傅俊伟[a,¥], 刘　敏[a,*]

[a]中南大学物理与电子学院, 湖南长沙410083, 中国
[b]慕尼黑大学物理学院, 慕尼黑, 德国
[c]郑州大学材料科学与工程学院, 河南郑州450052, 中国
[d]东京工业大学材料与化工技术学院, 材料与科学工程系, 东京, 日本

摘要: 过度的碳排放已造成了严重的全球环境问题, 电催化CO_2还原是一种利用间歇性过剩电能将CO_2转化为有价值的化学物质的有效策略. 在多种CO_2还原产物中, 二碳(C2)产物(如乙烯、乙醇)因其比一碳产物(如甲酸、甲烷、甲醇)具有更高的能量密度而备受关注. Cu是唯一能用电化学方法将CO_2转化为多碳产物的单金属催化剂. 如何提高Cu基催化剂上CO_2还原为C2产物的效率已引起了极大关注. 电催化还原CO_2生成C2产物有两个重要步骤: 一是参与碳碳偶联反应的CO*中

间体的量(*代表中间体吸附在基底表面), 二是碳碳偶联步骤的能垒. 对于Cu单金属催化剂, 虽然其表面碳碳偶联步骤的能垒相对较低, 但是Cu对CO_2的吸附能力和CO_2*加氢能力并不高, 导致在Cu表面不能生成足量的CO*中间体参与碳碳偶联反应, 因而对C2产物的选择性和活性并不理想. 与Cu单金属催化剂相反, 在Pd单金属催化剂表面, CO*中间体的形成具有超快的反应动力学, 但是CO*易在Pd表面中毒且后续碳碳偶联步骤的能垒极高, 使其表面不能生成C2产物. 为了充分发挥Cu(碳碳偶联步骤能垒较低)和Pd(CO*形成具有超快反应动力学)的双重优势, 本文构建了一种紧密的CuPd(100)界面, 以调节中间反应能垒, 从而提高C2产率.

密度泛函理论(DFT)计算表明, CuPd(100)界面增强了CO_2的吸附, 且降低了CO_2*加氢步骤的能垒, 从而能够催化生成更多的CO*中间体参与碳碳偶联反应. 且CuPd(100)界面上CO_2还原为C2产物的电位决定步骤能垒为0.61 eV, 低于Cu(100)表面的(0.72 eV).

本文采用了一种简便的湿化学法制备了CuPd(100)界面催化剂. X射线衍射和X射线光电子能谱测试以及扩展X射线吸收精细结构光谱结果表明, 合成的是相分离的CuPd双金属催化剂, 而非CuPd合金催化剂. 同时高分辨透射电镜可以观察到清晰的CuPd(100)界面. 由此可见, 本文成功合成了CuPd(100)界面催化剂. 程序升温脱附实验结果表明, CuPd(100)界面对CO_2和CO*的吸附比Cu强, 结果与理论预测一致. 气体传感实验结果表明, CuPd(100)界面CO_2*加氢能力比Cu强. 为评估CuPd(100)界面催化剂的催化活性, 进行了CO_2电化学还原实验. 结果表明, 在0.1 mol/L的$KHCO_3$电解液中, CuPd(100)界面催化剂在–1.4 V_{RHE}下, C2产物的法拉第效率为50.3% ± 1.2%, 是同电位下Cu催化剂的(23.6% ± 1.5%)的2.1倍, C2产物的选择性是Cu催化剂的2.4倍, 且具有更高的电流密度和更大的电化学活性面积. 本文通过调控中间反应能垒以合理设计铜基CO_2还原电催化剂提供了参考.

关键词: 二氧化碳电催化还原; 二碳产物; 铜钯界面催化剂; 中间反应能垒

收稿日期: 2020-11-18. 接受日期: 2020-12-09. 上网时间: 2021-05-05.

*通讯联系人. 电话: 13787082527; 电子信箱: minliu@csu.edu.cn

#通讯联系人. 电子信箱: xl_liu@csu.edu.cn

$通讯联系人. 电子信箱: mmiyauchi@ceram.titech.ac.jp

¥通讯联系人. 电子信箱: fujunwei@csu.edu.cn

基金来源: 国家自然科学基金(21872174, 22002189, 51673217, U1932148); 国家科技部重点研发国际间合作项目(2017YFE0127800, 2018YFE 0203402); 湖南省科技计划项目(2017XK2026); 湖南省自然科学基金(2020JJ2041, 2020JJ5691), 湖南省科技计划项目(2017TP1001); 深圳科技创新项目(JCYJ20180307151313532).

本文的电子版全文由Elsevier出版社在ScienceDirect上出版(http://www.sciencedirect.com/journal/chinese-journal-of-catalysis.